Ravi Nath Tiwari[1]
TPG,
University of Genoa,
Via Montallegro, 1,
Genova 16145, Italy
e-mail: ravinath.tiwari@edu.unige.it

Konstantinos Eleftheriou
LFMT,
Aristotle University of Thessaloniki,
Building D, Aristotle University Campus,
Thessaloniki 541 24, Greece
e-mail: elefthkd@auth.gr

Mario Luigi Ferrari
TPG,
University of Genoa,
Via Montallegro, 1,
Genova 16145, Italy
e-mail: mario.ferrari@unige.it

Theofilos Efstathiadis
LFMT,
Aristotle University of Thessaloniki,
Building D, Aristotle University Campus,
Thessaloniki 541 24, Greece
e-mail: theofil@auth.gr

Alberto Traverso
TPG,
University of Genoa,
Via Montallegro, 1,
Genova 16145, Italy
e-mail: alberto.traverso@unige.it

Anestis Kalfas
LFMT,
Aristotle University of Thessaloniki,
Building D, Aristotle University Campus,
Thessaloniki 541 24, Greece
e-mail: akalfas@auth.gr

Numerical Investigation of Bladeless Compressor on Different Disk Spaces and Diffuser Configurations

The cost-effectiveness of turbomachinery is a key aspect within the small-size compressor market. For this reason, Tesla turbomachinery, invented by Nikola Tesla in 1913, could be a good solution, particularly for low volumetric flow applications, where volumetric compressors are usually used. It consists of a bladeless rotor that stands out for its ease of construction and its ability to maintain almost the same performance as size decreases. One of its advantages is that it can run either as a turbine or as a compressor with minor modifications at the stator. The objective of this paper is to investigate a 3 kW Tesla compressor, which design was derived from an analogous Tesla expander prototype (58% isentropic efficiency from the numerical study), by conducting a computational fluid dynamic analysis for different disk gaps and diffuser configurations. The potential of the Tesla compressor is shown to be quite promising, with a peak isentropic efficiency estimated at 53%. Although bladeless compressor is a simple turbomachinery device, different parts, i.e., diffuser, tip clearance, and volute need to be optimized. Utilizing computational fluid dynamics algorithms, different disk gaps and different diffusers are simulated in order to increase the overall performance of the compressor and understand the flow dynamic behavior behind this technology. The dimensionless Ekman number is used to express the optimum disk space of the compressor rotor. Thus, the overall performance of the Tesla compressor is improved by 5–10% points compared to the initial model. Simultaneously, diffuser optimization strategies are applied and proved that there is a direct impact on the optimum design conditions, improving the pressure ratio at high mass flow rates. [DOI: 10.1115/1.4055705]

Keywords: Tesla turbomachinery, Ekman number, bladeless compressor

1 Introduction

The microscale compressor demand is increasing for microscale applications, i.e., power generation, medical, chemical processes, etc. The conventional compressor performance significantly decreases with decreased size, while it is almost constant for the bladeless turbomachinery. Nikola Tesla (1856–1943) is a famous scientist whose research and inventions are studied until now. Bladeless turbomachinery is the best of his inventions, according to his interview in 1912. Tesla filed his first patent in 1909. It was a boundary layer pump that was transferring energy to the fluid through multiple flat disks using viscous forces. Based again on the same principle, he managed to patent a turbine in 1911. Both boundary layer devices were accepted in 1913 [1,2] and took the name of their inventor. Until now, they are known as Tesla turbomachinery. Although Tesla turbomachinery is a revolutionary technology, it is not commercially applied to any industrial field due to its low performance.

It has been shown in several experiments that Tesla turbines have an isentropic efficiency of about 25% [3,4], with a peak efficiency of 36% [5], which is significantly lower than the theoretical one based on literature. However, Tesla turbomachinery has a variety of advantages such as simple design, low manufacturing cost, and the ability to run either as a turbine or as a compressor with minor changes. Furthermore, bladeless turbomachinery becomes a reasonable solution compared to conventional bladed impellers when scale-down design methods are applied [6]. This is mainly due to the constant performance of the first as size decreases. Thus, Tesla turbomachinery can be a potential prime mover for microgas turbines in the range of 200 W–3 kW [5].

The concept of running a Tesla turbine in reverse mode as a Tesla compressor is investigated in this paper. Tesla compressor consists of parallel flat corotating disks, mounted on a single shaft with the specified gap. Around the disks, there is a casing and several diffusers. The rotor causes the flow to enter through the center of the disks and exit from the multiple diffuser channels. Different gaps between the disks will be numerically analyzed and different diffuser configurations will be assessed. In this work, the original geometry of the existing expander prototype [5] is mildly changed to optimize the reverse compressor operation.

2 State-of-the-Art

There are several aerodynamic issues when a scaled-down component is designed. High rotational speed, which is a requirement to maintain the tip Mach number constant, creates vibration

[1]Corresponding author.

Manuscript received July 12, 2022; final manuscript received August 4, 2022; published online October 21, 2022. Editor: Jerzy T. Sawicki.

problems. The boundary layer thickness is comparable to the passage dimensions of the turbomachinery, increasing blockage and, as a result, affecting the efficiency [7]. Furthermore, the major loss mechanism in microturbomachinery is the viscous losses which are enhanced due to the low Reynolds number [8].

In the bladeless compressor, fluid viscosity is the main principle of transferring energy to the fluid [9]. The fluid is facing shear forces due to the rotation of the disk rotor and moves radially due to centrifugal forces. The fluid follows a path of an Archimedean spiral, and its size is proportional to the rotational speed. As a result, the fluid increases its total pressure while it reaches the diffuser part and then the volute.

The literature on Tesla compressors is quite limited. Generally, the first attempts were made in the direction of understanding the internal flow field. Crawford and Rice [10] found that the maximum performance of a Tesla pump occurred when the flow between the corotating disks is laminar. Boyd and Rice [11] split the flow field into two regions, the entrance and the asymptotic/Ekman regions. In the first one, the flow velocity profile is not fully developed while in the second one, the boundary layer is fully developed, as shown in Fig. 1. Breiter and Pohlhausen [12] created a model which calculates analytically the solution of the linearized governing equations. They assumed zero normal pressure gradient on the disk and low relative velocities. The model showed that the boundary layer profile is affected by the kinematic viscosity, the angular velocity, and the distance between the disks. Laroche and Ribaud [9] defined a parameter that contains all the previous variables, and it is called Ekman number. The complete equation of Ekman's number is given in Sec. 4.1. An analytical model is also created by Rice [13] assuming a two-dimensional flow between the disks.

Generally, these kinds of models were significantly weak to accurately estimate the flow parameters, especially in the asymptotic region. As a result, a few numerical analyses have been done in order to predict the performance of Tesla pumps and compressors. A finite difference method was applied by Boyd and Rice [11] to calculate the flow field between rotating disks, facing however issues in terms of high computational time. An integral method to define the flow parameters in the disk gap was chosen by Boyack and Rice [14]. This model had the same results as the one built by Boyd and Rice [11] with a reduced execution time. Further improvement in computational time of the integral method model was done by Crawford and Rice [10].

Aside from numerical or analytical models, bladeless compressors and pumps have also been experimentally investigated. Thus, a few experiments are conducted for corotating rotors, inlet geometries, diffusers, and volutes to assess the performance of the turbomachinery. Hasinger and Kehrt [15] tested experimentally a shear force pump. Pressure probes were used to measure the efficiency of the rotor. The model of the pump was created to measure the outlet pressure and changing rotational speed and mass flowrate. The measured efficiency was approximately 55%, lower than the one calculated using the analytical method. Rice [13] tested multiple-disk pumps and compressors. He also produced the performance map of the tested components. During his experiments, the maximum measured compressor efficiency was 21%, while the corresponding rotor efficiency predicted was 95%. Rice [16] assumed that this inconsistency was due to the diffuser configuration, something which is not confirmed yet. Almost all the bladeless pumps have been designed with simple methods based on empirical models. As a result, a large disk gap is implemented, leading to turbulence flow between the disk gaps [13,16].

In this paper, the performance of a bladeless turbine running in reverse mode is investigated. A University of Genova prototype 3 kW air Tesla turbine model is numerically studied as a Tesla compressor [5]. In this paper, existing model consider as the case 0 model and geometry details are shown in Table 1. The disk gap should be approximately twice the boundary layer thickness to maximize performance, where optimal Reynolds numbers are 5 or 6, based on Eq. (2) [16,18]. The Tesla rotor efficiency is determined for different disk spaces of the case 0 models, where the gap is optimized based on the Ekman number. The various cases are numerically tested using ANSYS FLUENT software. Table 1 shows the tested configurations, defining the four different geometrical rotor models (M1–M4).

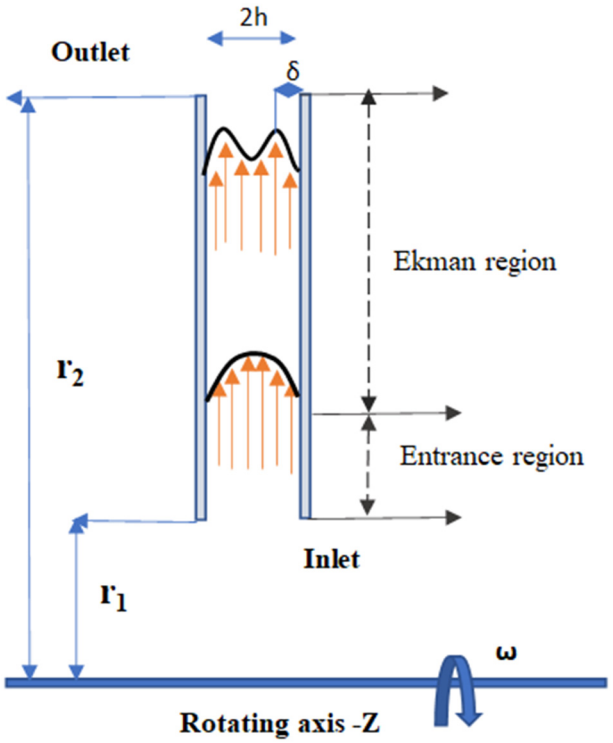

Fig. 1 Boundary layer profiles between two corotating disks

3 Numerical Methodology

With regards to the numerical analysis, ANSYS FLUENT provided two types of solvers, i.e., pressure-based and density-based. The pressure-based approach was developed initially for incompressible flow, while a density-based approach was used for high-speed compressible flow. However, both methods have now been extended to solve a wide range of flow conditions beyond their original capability [19,20]. Pressure-based solvers have demonstrated the capability to address highly compressible flows in turbomachinery applications, providing more computational stability than density-based solvers [17,19,21]. Therefore, a pressure-based steady solver is selected to solve the steady and compressible flow, with ideal gas as a working fluid in the current study [17]. The transition of laminar to turbulent or vice versa is not expected

Table 1 Design parameters of Tesla compressor

Design parameter	Size			
Model	M1	M2	M3	M4
Outer diameter (mm)	120			
Inner diameter (mm)	60			
Disks thickness (mm)	0.1			
Speed (rpm)	40,000			
Resulting parameter				
Ek	0.8	1.25	1.6	2
Gap (mm)	0.1	0.15	0.2	0.25
Renumber, $\omega(2\,h)r_1/\nu$ [17]	800	1201	1601	2001
Renumber, $\omega(2\,h)^2/\nu$ [16,18]	2.6	6.1	10.5	16.5
Disk numbers	120	96	80	69

in the Tesla rotor due to the very low Reynolds number. Moreover, the objective of the study captures the shear force in the rotor accurately. The three-dimensional Navier–Stokes equations are solved utilizing ANSYS FLUENT and discretized using the "finite volume method." The viscous model which is utilized is k–ω SST, a turbulence model which belongs to the Reynolds-averaged Navier–Stokes family and becomes the current industry standard for turbulence modeling [22]. The k–ω SST combines the better prediction of the k–ω model in the near-wall region with the k–ε model advantages in the far-field [23]. The flow between rotor and stator is turbulent due to the high velocity before the diffuser inlet. In order to cater to the requirement of $y+$ of the rotor and diffuser inlet, the k–ω SST model is used. k–ω SST model uses the equation based on the $y+$ value. It also considers the energy equation in order to take into account the heat transfer in the flow field. The viscous heating option is selected to consider the temperature change resulting from shear forces.

The governing equations are discretized using second-order upwind linear interpolation and solved using the COUPLED scheme for pressure and velocity coupling in fluent [20]. In this study, the flow domain between two rotating disks is considered stationary. For the entire "compressor-diffuser" configuration, half of the disk thickness and half of the gap rotating disks is considered as a single fluid domain shown in Fig. 2. This computational approach simplifies the problem, decreasing the execution time.

The numerical results are considered to be converged when the residuals of each solved equation are lower than 10^{-6}. Furthermore, the mass flowrate is one of the convergence criteria with an acceptable variation of less than 0.5%. At the same time, different flow parameters (i.e., inlet/outlet velocity and temperature) and mechanical parameters (torque and power), as well as flow field velocity and pressure contours, are continuously monitored in order to ensure that they are getting stable as the iteration number increases.

4 Tesla Rotor-Only Analysis

A computational fluid dynamic analysis was initially conducted in the rotor field only. This means that the numerical domain contains the area between two flat disks where the fluid governing equations are solved. The outcome of this analysis provides useful information for rotor-only features, in particular pressure ratio, isentropic efficiency that will later help to understand the rotor–diffuser coupled behavior.

4.1 Design Method. Table 1 shows the design parameters of the rotating disks. Based on the original prototype geometry (optimized for expander operation), the inner diameter of the compressor is 60 mm and the outer is 120 mm. The geometrical parameters, as well as the flow path, are illustrated in Fig. 1. Based on the literature [9,12], the main nondimensional parameter driving the boundary layer profile and as a result, the overall performance of two corotating bladeless rotors, is the Ekman number. The Ekman number is the ratio of the half-width of disk gap h and the boundary layer thickness δ, see Eq. (1). Based on literature there are two most used Reynolds number equations as shown in Eqs. (2) and (3). The first one is based on the disk gap [16,18] and the second one on the radius [17]

$$E_k = h/\delta = h\sqrt{\omega/\nu} \tag{1}$$

$$R_e = \frac{\omega(2h)^2}{\upsilon} \tag{2}$$

$$R_{e1} = \frac{\omega r_1 2h}{\upsilon} \tag{3}$$

The objective of this work is to find the optimum Ekman and Reynolds number for the Tesla compressor rotor. It is already known that the best efficiency appears when the Ekman number is between 1 and 2 [17]. This is the reason why the Ekman number is chosen to be 0.8, 1.25, 1.6, and 2 for the different design models, respectively. Wang et al. [17] chose Ekman number 2 for his analysis. The rotational speed is constant for every case in order to control the Ekman number by changing the gap between the disks. Reynolds number is also calculated for the different disk space rotor models to obtain the optimal configuration. It is expected that peak efficiency is reached when Reynolds is approximately 5 or 6 (Eq. (2)) [16,18]. Table 1 also shows the resulting Reynolds numbers calculated using Eqs. (2) and (3). This study focus on defining the optimal Ekman and renumbers of the bladeless compressor.

4.2 Mesh Dependency Analysis and Boundary Conditions. The "case 0" model and proposed Tesla compressor consists of eight diffusers; thus, a 45 deg-slice is simulated. Assuming axisymmetric flow, only half of the flow path is simulated, as shown in Fig. 2. Figure 2 also depicts the boundary conditions (i.e., inlet, outlet, moving wall, and periodic boundary conditions). A hexahedron grid is generated for the independent rotor analysis and tetrahedral mesh is chosen for the bladeless "rotor–diffuser" model analysis to discretize the computational domain. Furthermore, an inflation layer of four cells is applied close to the stationary and rotating wall regions, in order to refine the mesh and resolve accurately the boundary layer shape. The $y+$ is a nondimensional parameter that is important to see how accurately the boundary

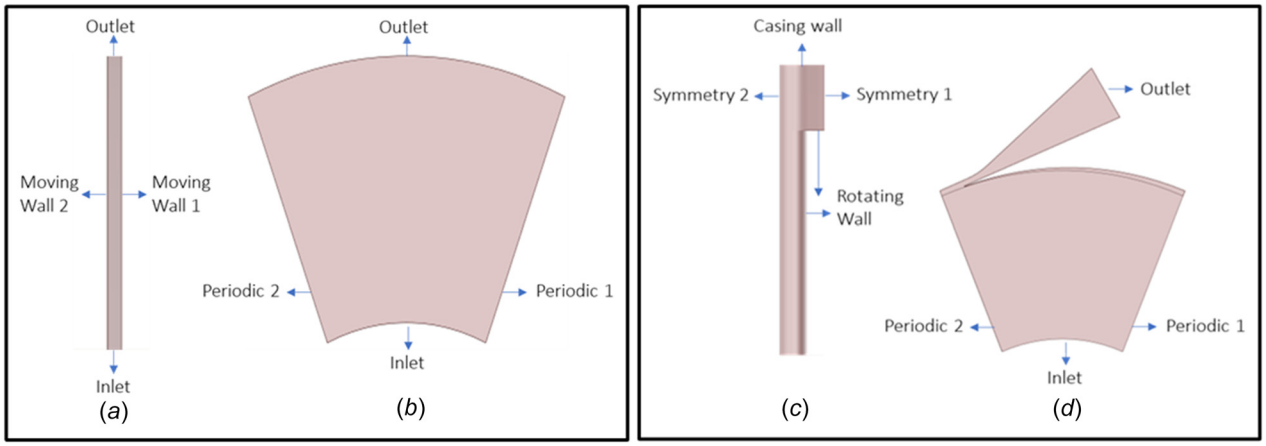

Fig. 2 Boundary conditions of the rotor-only (I) and diffuser analyses (II): (*a*) and (*c*) cross-sectional view and (*b*) and (*d*) front view

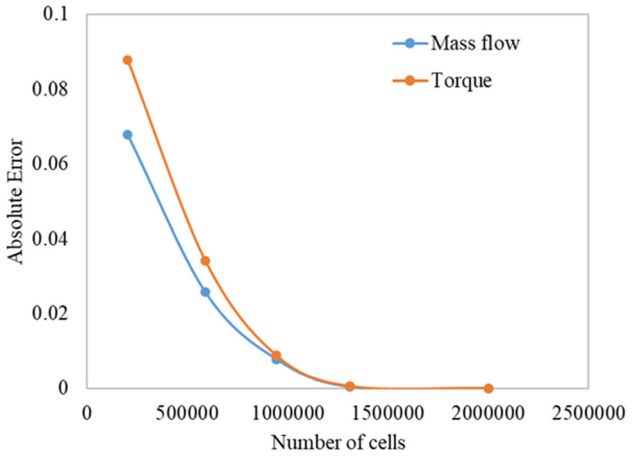

Fig. 3 Mesh convergence for mass flow and torque

layer is resolved. Two types of walls have been considered in analysis, first stationary and second rotating walls as shown in Fig. 2. A stationary wall is considered at diffuser where the average $y+$ value is less than 5 and a rotating wall is considered at rotor where $y+$ value is less than 1. In the k–ω SST model case, the facet average $y+$ value should be less than 5 is recommended for accuracy, and therefore in the current study, the average $y+$ value is maintained less than 5.

After conducting a mesh dependency analysis starting from 200,000 cells until 2,000,000 cells, an error of less than 0.1% is observed at mass flow and torque convergence (Fig. 3). Figures 4(*a*) and 4(*b*) show the generated mesh of the "rotor-only" and "case 0 bladeless compressor." The analysis is conducted with a mesh of 1,310,000 cells which corresponds to an error of 0.05% for torque and mass flow variables and this mesh size is selected for the present study.

The boundaries conditions at inlet/outlet are set as total pressure inlet and mass flow outlet [22,24]. The total pressure of 101,325 kPa and total temperature of 300 K are applied at the inlet while different mass flow rates are assigned at the outlet. With regards to walls, nonslip condition and adiabatic options are selected.

4.3 Performance Analysis. In the "rotor-only" analysis, emphasis is given to total-to-total quantities. To calculate total pressure and total-to-total adiabatic efficiency, Eqs. (4) and (5) are used. The flow parameters at the inlet and outlet are mass flow averaged in order to calculate the compressor's overall performance (Fig. 5(*a*))

$$\mathrm{PR} = \frac{p_{t2}}{p_{t1}} \tag{4}$$

$$\eta_{t-t} = \dot{m}\, C_P\, T_{t1}\, \frac{\mathrm{PR}^{\frac{k-1}{k}} - 1}{\tau\, \omega} \tag{5}$$

Figure 5(*a*) shows the total to total and static to static pressure ratio lines for four different Ekman numbers. The characteristic line of Ekman number equal to 1.6 is higher compared to the other cases in all mass flow rates. At the same time, the total-to-total adiabatic efficiency is higher at Ekman number 1.6 (Fig. 5(*b*)). In the tested cases, the Reynolds number is around 10 (Fig. 6), almost double than optimal 5 and 6 [16,18]. The rotor model (M1) shows the lowest efficiency of around 78% at 0.8 Ekman number. Figure 6 shows an efficiency increase with rising the Ekman number until 1.6. Thus, the performance map clearly shows that Ekman number around 1.6 is the optimum case, especially for low mass flow rates where "rotor-only" total to total efficiency is more than 82.6%. Around a 5% efficiency increase is shown between

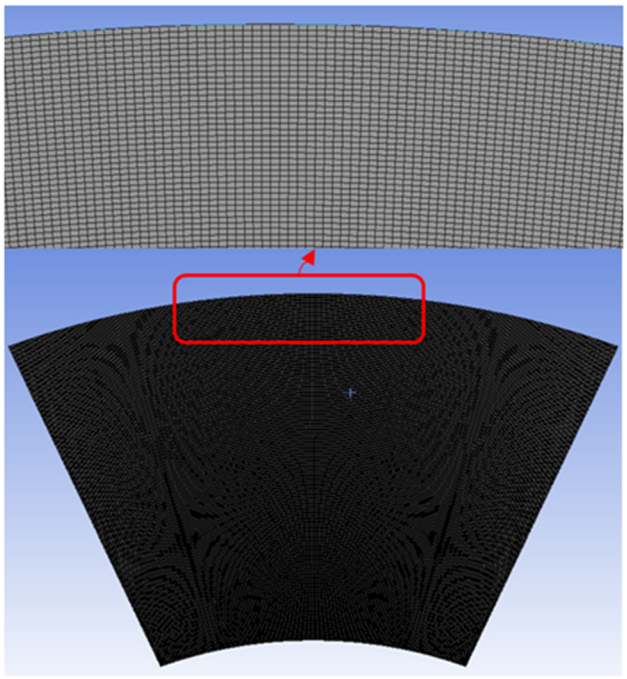

(*a*)

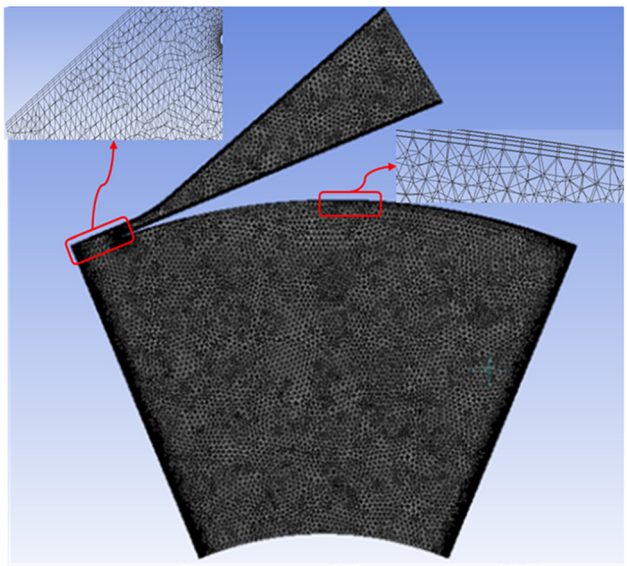

(*b*)

Fig. 4 (*a*) Generated mesh: rotor-only analysis and (*b*) generated mesh: Tesla compressor geometry "case 0"

model M1 (Ek-0.8) and rotor model M3 (Ek-1.6). The static–static pressure versus mass flow is shown in Fig. 5(*a*) where Ekman 1.6 indicates a higher static pressure ratio of 1.29 compared to other Ekman numbers at 0.045 g/s. The analysis is carried out for the single gap and the higher efficiency is obtained at 0.045 g/s. Increasing the disk gap that in comparing the characteristic lines of the rotor-only Tesla compressor to the conventional one, there is a different behavior. It is apparent that in our case, the pressure ratio line is asymptotic to the y-axis while in the bladed compressor is asymptotic to the x-axis. This outcome is quite interesting and it actually explains the advantage of bladeless turbomachinery. Due to the lack of blades, the flow can adapt to the optimal flow angle at different mass flow rates, giving each time the highest performance. This obviously cannot happen in a

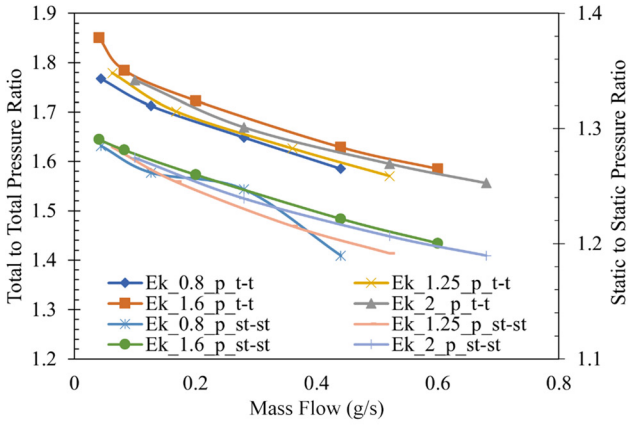

(*a*)

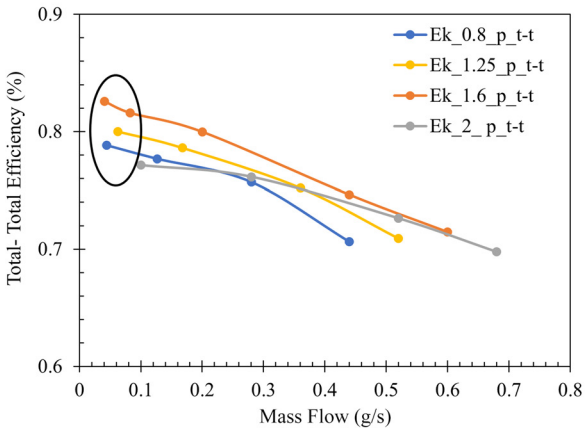

(*b*)

Fig. 5 (*a*) Rotor-only total–total and static–static pressure ratio versus mass flowrate for different Ekman numbers and (*b*) rotor-only total to total adiabatic efficiency versus mass flowrate for different Ekman numbers

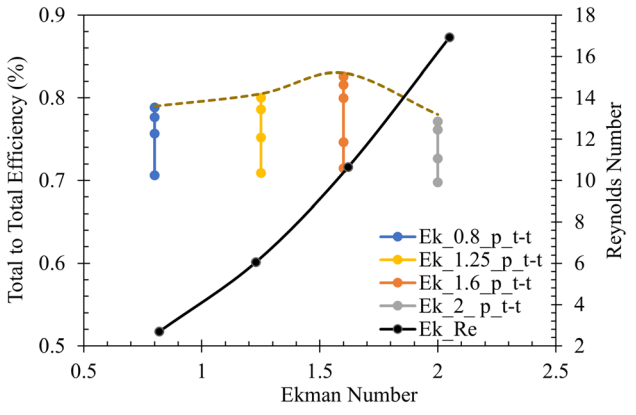

Fig. 6 Rotor-only total to total adiabatic efficiency and Reynolds number versus Ekman number (Ek-0.8–1.6 worst-best and Ek-1.6–2 best-worst)

constant blade compressor where losses decrease the performance as we diverge from the operating point.

Based on the numerical analysis, the flow angle is calculated to be equal to 89.88 deg Eq. (6) at 0.045 g/s mass flowrate, where the total to isentropic efficiency is 82.6%. Wang et al. [17] is calculated the flow angle at 89.5 deg where isentropic efficiency is 83%

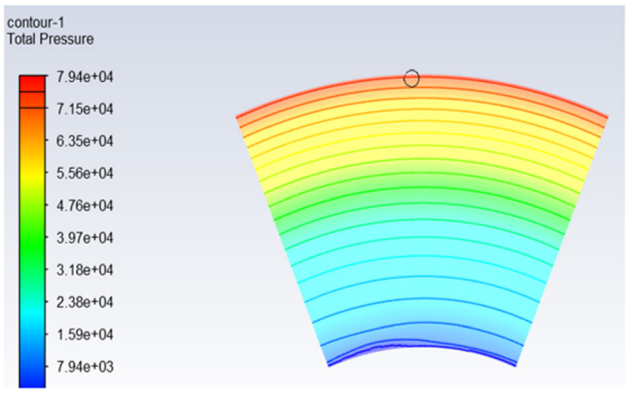

Fig. 7 Rotor-only total pressure contour for Ekman number = 0.8—gap = 0.1 mm (M1), mass flow = 0.045 g/s

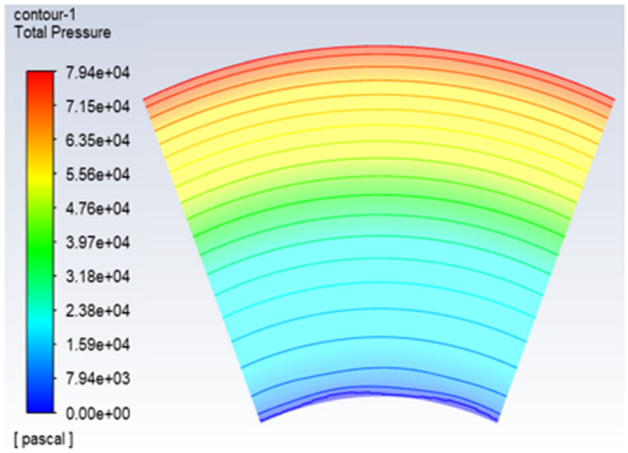

Fig. 8 Rotor-only total pressure contour for Ekman number = 1.6—gap = 0.2 mm (M3), mass flow = 0.045 g/s

$$\tan(\alpha_2) = \frac{V_{t2}}{V_{r2}} \tag{6}$$

For an insight into the main flow phenomena, Ekman numbers of 0.8–1.6 indicate the worst-to-best cases, and Ekman numbers of 1.6–2 indicate the best-to-worst cases. In both cases (Figs. 7 and 8), the smooth increase of the total pressure can be observed, however, the higher Ekman number case shows a higher gradient. This means momentum can be transferred more effectively to the flow in this case.

5 Diffuser Design

There are several challenges in designing the Tesla compressor to improve its performance. The stator design is quite significant and is affected by a number of parameters, i.e., diffuser angle, shape, diffuser length, area ratio, clearance between diffuser and rotor. There is no specific data available to design the Tesla compressor stator. According to Rice [13], the stator/diffuser needs to be placed in a direction almost tangential to the rotor disks. However, this has not been proven yet. It is recognized that in bladeless machinery significant losses occur in the interaction [17].

In this section, starting from the original "case 0" geometry of the stator and two new diffuser configurations cases 1 and 2 are proposed as shown in Table 2. The rotor–stator interaction gab is in average 0.5 mm, it is the same for all tested cases and it is not an optimization parameter for this study. Furthermore, only the rectangular diffuser type is considered. In "case 0," the diffuser

Table 2 Design parameters of diffuser

Model	No. of diff.	Throat (mm)	Exit (mm)	Length (mm)	Diff. angle (deg)	Divergent angle (deg)
Case 0	8	1.00	10.20	31	2.30	18.50
Case 1	8	1.31	4.76	40	5.00	4.10
Case 2	8	1.10	3.00	45	3.50	2.40

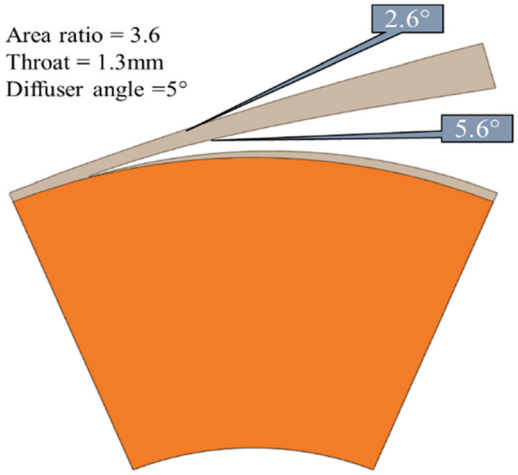

Fig. 9 Proposed diffuser case 1 with rotor model M3 (Ek-1.6)

has an area ratio of 10.2 with a divergent angle of 18.5 deg while the diffuser is placed at a 2.3 deg angle. In "case 1," the diffuser is a bent channel with an area ratio of 3.6 where the throat is 1.3 mm. The diffuser is placed at a 5 deg angle and its upper and lower sections are diverted by 2.6 deg and 5.6 deg (average 4.1 deg), respectively, as shown in Fig. 9. The second proposed (case 2) diffuser is a straight channel with a throat of 1.1 mm, an area ratio of 2.7, a diffuser angle of 3.5 deg and a divergent angle of 2.4 deg illustrated in Fig. 10. The width is kept the same in all diffuser cases. According to standard maps for a linear diffuser with a rectangular cross section [25,26], the "case 0" diffuser lies outside, which shows the recirculation as visualized in Fig. 11(*b*). This diffuser was designed for the expander model; hence an improved design of the diffuser is needed. The "case 1" and "case 2" diffusers are fulfilling the requirement of standard linear diffuser maps and increase the performance of the compressor.

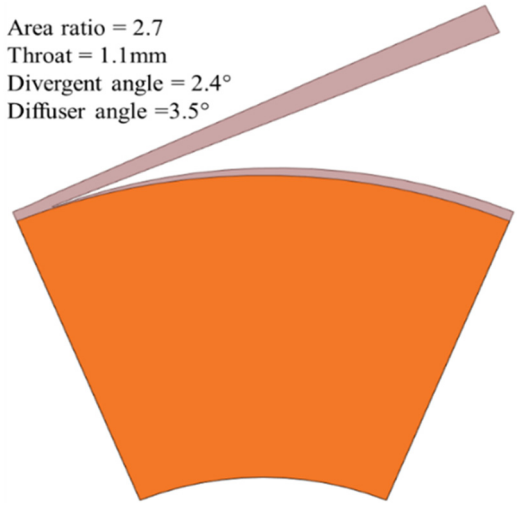

Fig. 10 Proposed diffuser case 2 with rotor model M3 (Ek-1.6)

Based on the literature, the second proposed diffuser configuration (case 2) is expected to have better performance due to the higher-pressure recovery [25].

6 Results

The combination of rotor–diffuser configuration is simulated at a rotational speed of 40 krpm. First, the "case 0" model of the Tesla expander running in reverse mode is assessed and aligned with the original prototype. Then, the same rotor, operated in reverse rotational speed and coupled alternatively to one of the two new diffusers, is numerically investigated. The simulation is steady-state, and the performance characteristics are calculated based on mass flow averaged numerical results at the inlet/outlet of the Tesla compressor.

Figure 12 presents the total to static pressure ratio as a function of mass flowrate for the three diffuser configurations (cases 0,1, and 2). Pressure ratio decreases with the mass flow increase as expected, the rotor model M3 (Ek-1.6) presents the highest static

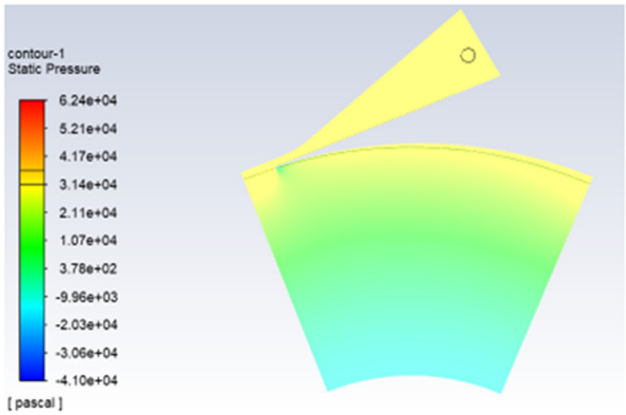

(*a*)

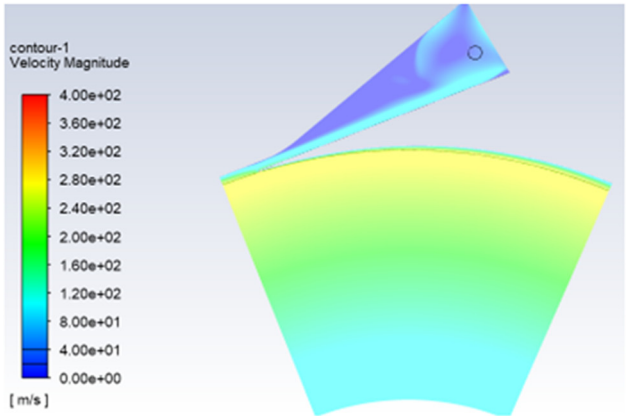

(*b*)

Fig. 11 (*a*) Static pressure contours for case 0 prototype geometry (Ek-1.6, mass flow-0.49 g/s) and (*b*) velocity contours for case 0 prototype geometry (case 0, Ek-1.6, mass flow-0.49 g/s)

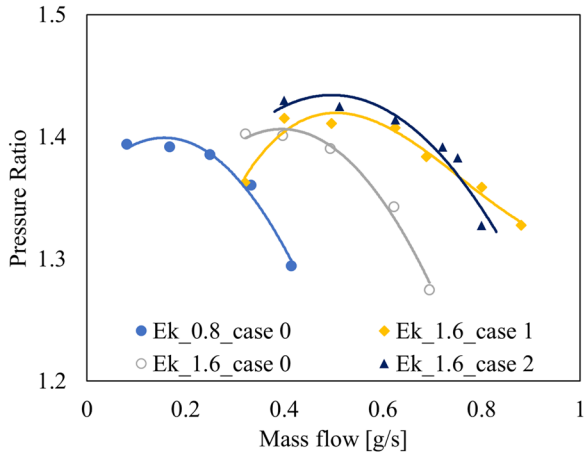

Fig. 12 Total to static pressure ratio versus mass flowrate for different compressor configurations

to static 1.29 and total to total 1.85 pressure ratio at low mass flow 0.045 g/s as shown in Fig. 5(*b*), where rotor efficiency is 82.6%. The total-static pressure ratio obtained for "case 2" is 1.45. However, the characteristic curve of the Tesla compressor with the second proposed diffuser "case 2" shows higher pressure ratios compared to other configurations. The better performance is achieved at a low mass flowrate for all three diffuser configurations. It is quite important to mention the drop of the pressure ratio due to the existence of the diffuser. Rotor-only analysis shows that the total to total pressure ratio can reach up to 1.8 at low at mass flow for model M3 (Ek = 1.6, gap 0.2). M3 model is tested with both proposed diffusers cases 1 and 2, and total to static pressure ratio is found 1.41 for the first diffuser "case 1" and 1.45 for the second "case 2" at the mass flowrate of 0.045 g/s (Fig. 12). The overall analysis is carried out based on the single disk gap.

Apart from the pressure ratio, total to static efficiency is also calculated for the "rotor–diffuser" configurations. Figure 13 presents the produced results, the efficiency curve of the "case 2" diffuser stands out compared to the other two cases 0 and 1. Maximum efficiency appears at 0.4 g/s and is 53% for the case 2 diffuser–rotor model (M3-Ekman 1.6) The case 0 configuration has again the lowest efficiency while the first configuration floats between the rest. Considering the model (M1) of rotor-only analysis, the total to total efficiency at 0.4 g/s is 70.6%, while model M3 is 75%.

Having a closer observation on the computational fluid dynamic results and specifically on the static pressure and velocity contours

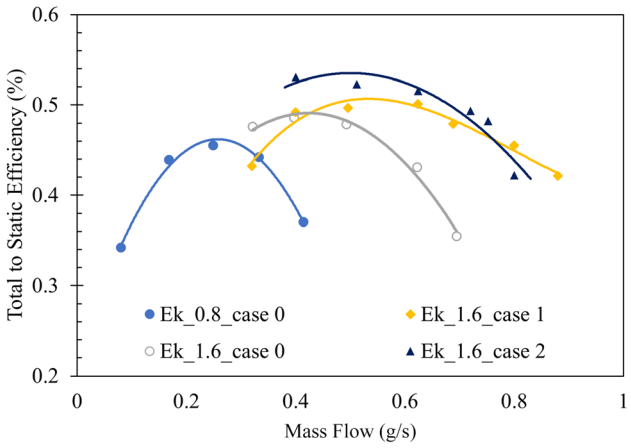

Fig. 13 Total to static efficiency versus mass flowrate for different compressor configurations

in Figs. 11 and 14, the shape of the performance line can be explained. With regards to the case 0 configuration, a massive recirculation area appears at the exit of the diffuser. The diffuser divergence angle is way far from the ideal values, making the flow to separate. The second diffuser has a better performance. Its wall angles are in the optimum design range. However, at the exit of the first diffuser configuration, a jet-wake flow is observed. Moreover, the area covered by the wake flow is almost the same as the area of the jet. The absence of a separation bubble makes that configuration better than the case 0. Figures 11(*a*) and 11(*b*) show the static pressure and velocity fields of the best-tested configuration at 0.49 g/s mass flow. The diffuser design must have a direct impact on the performance characteristics of the Tesla compressor. The "case 0" shows a huge recirculation in the diffuser which is minimized in case 1 and further minimize in case 2 diffuser as shown in Figs. 14(*a*) and 14(*b*). Figure 14(*b*) shows the velocity differences in the upper and lower region at the exit of the diffuser. The velocity field at the exit of the diffuser is more uniform, limiting the separation losses. A reduced area of wake flow still exists at the top wall of the diffuser. However, this is because of the velocity profile entering the diffuser. The upper and the lower walls of the diffuser are located at different radii, thus, the profile is not constant, resulting in the confined jet-wake outlet profile. The implementation of model M3 (Ek-1.6) will

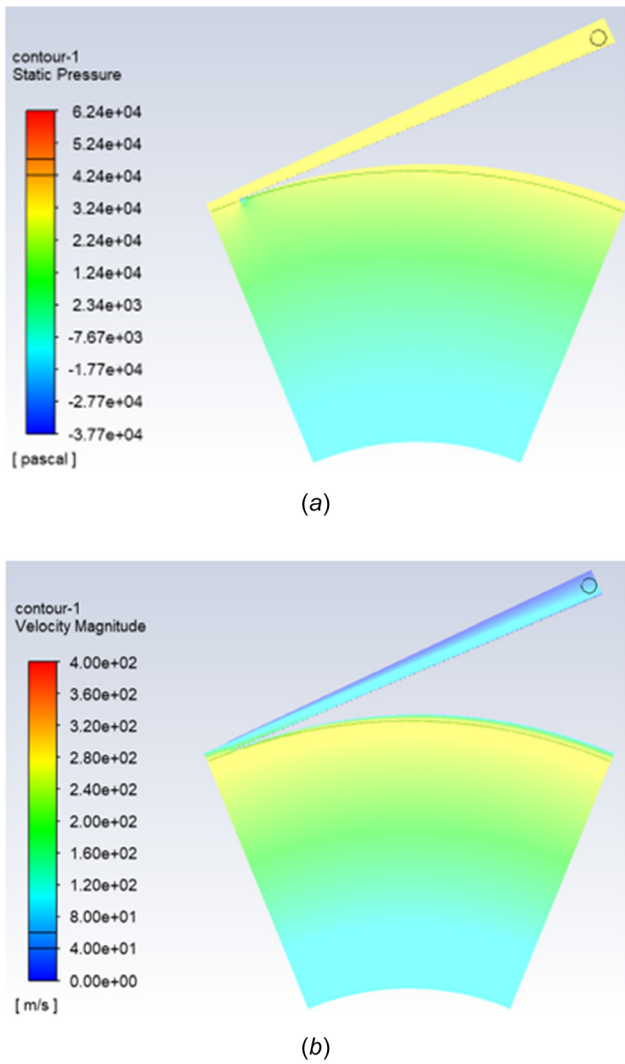

Fig. 14 (*a*) Static pressure for proposed diffuser (case 2, Ek-1.6, mass flow = 0.49 g/s) and (*b*) velocity contours for proposed diffuser (case 2, Ek-1.6, mass flow = 0.49 g/s)

benefit in the overall performance and reduce the number of disks by 33% as shown in Table 1 and as a result the production cost.

7 Conclusion

This paper investigates numerically the performance of the Tesla compressor based on a case 0 prototype geometry by analyzing the flow phenomena between two corotating disks. Initially, an independent rotor analysis is performed to determine which is the most suitable Ekman number for maximum performance. After that, two shapes of diffusers are proposed. And finally, three rotor–diffuser configurations are numerically tested, and their results were compared with the outputs of the "rotor-only" analysis. The following main results are found in the present study:

- The rotor-only analysis shows that the axial distance between two disks significantly influences Tesla compressor performance: peak performance is found at Ekman number 1.6, where the optimal Reynolds number is 10, and the disk gap is three times of the boundary layer thickness.
- A new characteristic line shape of the rotor-only test is found, due to the self-corrected flow angle of the fluid.
- Among the rotor models, M3 showed higher efficiency of over 82.5%. The rotor model M1 showed 5% less efficiency than M3, so replacing M1 with M3 will result in a reduction of 33% of the disk and the disk gap of the prototype rotor model "case 0."
- The rotor–stator computational analysis reveals that in order to use a Tesla turbine in reverse mode (as Tesla compressor), the diffuser needs to be modified. Moreover, results show that the second proposed diffuser "case-2" configuration has better performance in total to static and static to static pressure ratio. The overall efficiency obtained 53% at 0.40 g/s mass flow for the M3 rotor and "case 2" stator model, while rotor model M1 "case 0" diffuser is 36% at 0.40 g/s.
- The nonuniform velocity profile at the inlet of the diffuser directly affects the performance of the diffuser and the overall performance of the Tesla compressor.

Acknowledgment

This project has received funding from the European Union's Horizon 2020 research and innovation programme under the Marie Sklodowska-Curie Grant Agreement No. 861079 ("NextMGT—Next Generation of Micro-Gas Turbines for High Efficiency, Low Emissions, and Fuel Flexibility"). This paper reflects only the authors' view and the Research Executive Agency and the European Commission are not responsible for any use that may be made of the information it contains.

Nomenclature

C_p = isobaric specific heat, kJ/kg K
Ek = Ekman number
k = specific heat ratio
$\dot{m}$ = mass flow rate, g/s
N = rotational speed, krpm
P = power, W
p_{t1} = inlet total pressure, Pa
p_{t2} = outlet total pressure, Pa
r_1 = inner radius, mm
r_2 = outer radius, mm
Re = Reynolds number
t = disk thickness, mm
T_{t1} = inlet total temperature, K
V_r = radial velocity
V_t = tangential velocity
$2h$ = disk gap, mm
α_2 = flow angle, deg
δ = boundary layer thickness, mm
η = efficiency
ν = kinematic viscosity, m^2/s
τ = torque, N·m
ω = angular velocity, rad/s

Subscripts

st–st = static to static
t–t = total to total

Acronyms

CFD = computational fluid dynamics
PR = pressure ratio

References

[1] Tesla, N., 1913, "Turbine," U.S. Patent No. 1,061,206.
[2] Tesla, N., 1913, "Fluid Propulsion," U.S. Patent No. 1,061,142.
[3] Rice, W., 1965, "An Analytical and Experimental Investigation of Multiple Disk Turbines," ASME J. Eng. Power, **87**(1), pp. 29–36.
[4] Lemma, E., Deam, R., Toncich, D., and Collins, R., 2008, "Characterisation of a Small Viscous Flow Turbine," Exp. Therm. Fluid Sci., **33**(1), pp. 96–105.
[5] Renuke, A., Reggio, F., Silvestri, P., Traverso, A., and Pascenti, M., 2020, "Experimental Investigation on a 3 kW Air Tesla Expander With High-Speed Generator," ASME Paper No. GT2020-14572.
[6] Epstein, A. H., 2004, "Millimeter-Scale, Micro-Electro-Mechanical Systems Gas Turbine Engines," ASME J. Eng. Gas Turbines Power, **126**(2), pp. 205–226.
[7] Beans, E. W., 1961, "Performance Characteristics of a Friction Disk Turbine," Ph.D. thesis, The Pennsylvania State University, State College, PA.
[8] Sirakov, B. T., Gong, Y., Epstein, A. H., and Tan, C. S., 2004, "Design and Characterization of Micro-Compressor Impellers," ASME Paper No. GT2004-53332.
[9] Laroche, E., and Ribaud, Y., 1999, "An Analysis of the Internal Aerodynamic Losses Produced in the Laminar and Centrifugal Flow Between Two Parallel Co-Rotating Disks," Proceedings of the 3rd European Conference on Turbomachinery: Fluid Dynamics and Thermodynamics, V. B. Proceedings, London, UK, Mar. 2–5, IMechE Conference Transaction, No. 1999-1B, p. 1112, Paper No. C557/001/99.
[10] Crawford, M. E., and Rice, W., 1974, "Calculated Design Data for the Multiple-Disk Pump Using Incompressible Fluid," ASME J. Eng. Power, **96**(3), pp. 274–282.
[11] Boyd, K. E., and Rice, W., 1968, "Laminar Inward Flow of an Incompressible Fluid Between Rotating Disks With Full Peripheral Admission," ASME J. Appl. Mech., **35**(2), pp. 229–237.
[12] Breiter, M. C., and Pohlhausen, K., 1962, "Laminar Flow Between Two Parallel Rotating Disks," Aeronautical Research Laboratories, Wright-Patterson Air Force Base, OH, Technical Report No. ARL 62–318.
[13] Rice, W., 1963, "An Analytical and Experimental Investigation of Multiple Disk Pumps and Compressors," ASME J. Eng. Power, **85**(3), pp. 191–198.
[14] Boyack, K. E., and Rice, W., 1971, "Integral Method for Flow Between Corotating Disks," ASME J. Basic Eng., **93**(3), pp. 350–354.
[15] Hasinger, S. H., and Kehrt, L. G., 1963, "Investigation of a Shear Force Pump," ASME J. Eng. Power, **85**(3), pp. 201–206.
[16] Rice, W., 2003, "Tesla Turbomachinery," *Handbook of Turbomachinery*, Vol. 14, E. Logan, and R. Roy, eds., Marcel Dekker, New York.
[17] Wang, B., Okamoto, K., Yamaguchi, K., and Teramoto, S., 2014, "Loss Mechanisms in Shear-Force Pump With Multiple Corotating Disks," ASME J. Fluids Eng., **136**(8), p. 081101.
[18] Oliveira, M., and Pascoa, J. M., 2009, "Analytical and Experimental Modeling of a Viscous Disk Pump for MEMS Applications," III National Conference on Fluid Mechanics, Thermodynamics and Energy, MEFTE-BRAGANÇA 09, Braganca, Portugal, Sept. 17–18, Vol. 9.
[19] Zhu, Y., and Jiang, P., 2014, "Experimental and Numerical Investigation of the Effect of Shock Wave Characteristics on the Ejector Performance," Int. J. Refrig., **40**, pp. 31–42.
[20] Galindo, J., Hoyas, S., Fajardo, P., and Navarro, R., 2013, "Set-Up Analysis and Optimization of CFD Simulations for Radial Turbines," Eng. Appl. Comput. Fluid Mech., **7**(4), pp. 441–460.
[21] Croquer, S., Poncet, S., and Aidoun, Z., 2016, "Turbulence Modeling of a Single-Phase R134a Supersonic Ejector. Part 1: Numerical Benchmark," Int. J. Refrig., **61**, pp. 140–152.
[22] Dewar, B., Tiainen, J., Jaatinen-Värri, A., Creamer, M., Dotcheva, M., Radulovic, J., and Buick, J. M., 2019, "CFD Modelling of a Centrifugal Compressor With Experimental Validation Through Radial Diffuser Static Pressure Measurement," Int. J. Rotating Mach., **2019**, pp. 1–12.
[23] Menter, F. R., 1992, "Influence of Freestream Values on k-Omega Turbulence Model Predictions," AIAA J., **30**(6), pp. 1657–1659.
[24] Elyamin, G. R. A., Bassily, M. A., Khalil, K. Y., and Gomaa, M. S., 2019, "Effect of Impeller Blades Number on the Performance of a Centrifugal Pump," Alexandria Eng. J., **58**(1), pp. 39–48.
[25] Schmandt, B., and Herwig, H., 2011, "Diffuser and Nozzle Design Optimization by Entropy Generation Minimization," Entropy, **13**(7), pp. 1380–1402.
[26] Obayashi, S., Jeong, S.-K., Shimoyama, K., Chiba, K., and Morino, H., 2010, "Multi-Objective Design Exploration and Its Applications," Int. J. Aeronaut. Space Sci., **11**(4), pp. 247–265.